UMYU Scientifica, Vol. 5 NO. 1, March 2026, Pp 391 – 401
https://doi.org/10.56919/usci.2651.033
ISSN: 2955 – 1145 (print); 2955 – 1153 (online)
A periodical of the Faculty of Natural and Applied Sciences, UMYU, Katsina

ORIGINAL RESEARCH ARTICLE

Simulation-Based Performance Analysis of a 50-km Optical Fiber Link Under Increasing Data Rates

Abdurrasheed B. Magaji[1]* and Sada Y. Aliyu[2]
[1]Department of Physics, Faculty of Natural and Applied Sciences, Umaru Musa Yar'adua University, Katsina, Nigeria
[2]Department of Basic and Applied Sciences, Hassan Usman Katsina Polytechnic, Katsina, Nigeria

ABSTRACT
The exponential growth in data traffic necessitates high-performance optical communication systems capable of operating at elevated data rates while maintaining signal integrity. This study presents a comprehensive simulation-based performance analysis of a 50 km single-mode fiber (SMF) optical communication link using OptiSystem version 18.0. Six key performance metrics eye opening, signal-to-noise ratio (SNR), bit error rate (BER), quality factor (Q-factor), eye closure penalty, and dispersion penalty were evaluated as functions of data rate ranging from 5 Gbit/s to 25 Gbit/s. Results demonstrate non-linear degradation with increasing data rate. The Q-factor decreased from 12.67 to 3.95, SNR degraded from 22.0 dB to 11.0 dB, and BER increased from approximately 10^{-12} to 10^{-3}. Eye diagram analysis at representative data rates of 5, 15, and 25 Gbit/s revealed progressive eye closure corresponding to a 77.5% reduction in eye opening. The analysis identifies a critical threshold at 16 Gbit/s where performance deteriorates rapidly due to dispersion-induced inter-symbol interference. For the studied configuration, error-free transmission (BER < 10^{-12}) requires operation below 16 Gbit/s, while forward error correction (FEC) allows operation up to approximately 24 Gbit/s. These results provide practical design guidelines for optimizing data rate selection in 50 km SMF optical links using OptiSystem simulation.

ARTICLE HISTORY
Received December 01, 2025
Accepted March 13, 2026
Published March 28, 2026

KEYWORDS
Optical fiber communication, data rate, bit error rate, Q-factor, eye diagram, signal-to-noise ratio, OptiSystem simulation, dispersion penalty, chromatic dispersion, inter-symbol interference

INTRODUCTION
Optical fiber communication forms the backbone of modern global communication networks due to its high bandwidth capacity and low transmission loss. Increasing demand for broadband services such as high-definition video streaming, cloud computing, and fifth-generation (5G) wireless networks requires optical communication systems to operate at progressively higher data rates. However, increasing the transmission data rate introduces several impairments that degrade signal integrity. These impairments include chromatic dispersion, polarization mode dispersion, nonlinear optical effects, and receiver noise. As the bit rate increases, pulse broadening caused by chromatic dispersion leads to inter-symbol interference (ISI), which reduces the eye opening of the received signal and increases the bit error rate.

To evaluate the performance of optical communication systems, several metrics are commonly used, including the eye diagram, signal-to-noise ratio (SNR), bit error rate (BER), and quality factor (Q-factor). The eye diagram provides a visual representation of signal integrity, where a wider eye opening indicates lower noise and reduced inter-symbol interference. The relationship between BER and Q-factor for Gaussian noise statistics is given by the complementary error function (Ramaswami et al., 2016; Essiambre & Tkach, 2008; Senior & Jamro, 2009). While extensive research has examined individual performance metrics, a significant gap exists in the literature regarding integrated, simultaneous analysis of eye opening, SNR, BER, Q-factor, eye closure penalty, and dispersion penalty across a standardized link configuration. Previous studies have typically focused on one or two metrics in isolation (Winzer & Essiambre, 2006; Kikuchi, 2016; Liu, 2017; Xu & Sillard, 2020). Furthermore, most published work lacks comprehensive numerical datasets that enable direct application to link budget calculations.

This study addresses the identified gap by presenting a comprehensive multi-metric analysis of a 50 km single-mode fiber (SMF) link operating over a data rate range of 5–25 Gbit/s. Its key contribution lies in the integration of six performance metrics into a unified framework, allowing simultaneous evaluation of all critical system indicators. In addition, the study provides a complete numerical dataset suitable for direct engineering

Correspondence: Abdurrasheed B. Magaji. Department of Physics, Faculty of Natural and Applied Sciences, Umaru Musa Yar'adua University, Katsina, Nigeria. ✉ abdulrasheed.magaji@umyu.edu.ng.
How to cite: Magaji, A. B., & Aliyu, S. Y. (2026). Simulation-Based Performance Analysis of a 50-km Optical Fiber Link Under Increasing Data Rates. *UMYU Scientifica*, 5(1), 391 – 401. https://doi.org/10.56919/usci.2651.033

application, identifies a critical performance threshold at 16 Gbit/s through quantitative analysis, and develops practical design guidelines to support optimization of 50 km SMF communication links.

The objectives of this study are to systematically quantify the relationship between data rate and six key performance metrics, namely eye opening, signal-to-noise ratio (SNR), bit error rate (BER), Q-factor, eye closure penalty, and dispersion penalty. It also aims to present eye diagram visualizations at representative data rates of 5, 15, and 25 Gbit/s to illustrate system behavior under varying conditions. Furthermore, the study seeks to analyze the underlying degradation mechanisms affecting system performance and to identify critical thresholds beyond which performance significantly deteriorates. Finally, it aims to translate these findings into practical design guidelines for optimizing the performance of 50 km SMF links.

1.1 Fundamental Performance Metrics in Optical Communication

To ensure reliable communication, system performance is quantified using specific indicators. The Eye Diagram provides a qualitative and quantitative view of signal integrity, where the vertical eye opening is directly related to the noise margin, and the eye width indicates timing jitter and inter-symbol interference (ISI) susceptibility (Jargon et al., 2005; Sharma & Singh, 2020). The eye closure penalty (ECP) quantifies signal degradation relative to a reference condition:

$$ECP(dB) = 10log_{10}(\frac{Eye\ Opening_{references}}{Eye\ Opening_{measured}}) \quad (1)$$

The Signal-to-Noise Ratio (SNR) measures signal power relative to noise power at the receiver decision circuit. For optical systems, the electrical SNR is expressed as:

The **Signal-to-Noise Ratio (SNR)** measures signal power relative to noise power at the receiver decision circuit. For optical systems, the electrical SNR is expressed as:

$$SNR_{dB} = 10log_{10}\left(P_{signal}/P_{noise}\right) = 10log_{10}(\frac{V_1-V_0}{\sigma_1^2+\sigma_0^2}) \quad \ldots \quad (2)$$

Poggiolini (2012) demonstrated that the relationship between SNR and BER is inverse and exponential; a small decrease in SNR can lead to several orders of magnitude increase in BER.

The **Bit Error Rate (BER)** is the definitive measure of system accuracy, defined as the probability of incorrect bit identification. For On-Off Keying (OOK) modulation with Gaussian noise statistics and optimized decision threshold, the BER is related to the Q-factor by (Personick, 1973; Smith & Personick, 1980):

$$BER = \frac{1}{2}\ erfc(\frac{Q}{\sqrt{2}}) \quad (3)$$

The **Quality Factor (Q-Factor)** bridges SNR and BER, providing a direct method to estimate link health without time-consuming BER counting at low error rates (Bergano et al., 1993; Freund et al., 2011). It is defined as:

$$Q = \frac{V_1-V_0}{\sigma_1+\sigma_0} \quad (4)$$

For $Q > 3$, Equation (3) can be approximated as:

$$BER \approx exp\frac{(-Q^2/2)}{Q\sqrt{2\pi}} \quad (5)$$

The **Dispersion Penalty** quantifies the degradation due to chromatic dispersion. The pulse broadening (ΔT) is given by (Chraplyvy, 1990; Bellotti et al., 1999):

$$\Delta T = D.L.\Delta\lambda \quad (6)$$

where D is the dispersion coefficient, L is the fiber length, and $\Delta\lambda$ is the source spectral width. The dispersion penalty in dB can be expressed as:

$$P_{disp}(dB) = 10log_{10}(\frac{\Delta T}{T_b}) \quad (7)$$

where $T_b = \frac{1}{R_b}$ is the bit period when ΔT exceeds a significant fraction of T_b severe ISI occurs, closing the eye and increasing BER.

1.2 Data Rate Limitations and Noise Considerations

Increasing the data rate necessitates wider receiver bandwidth, which directly impacts noise performance. The receiver noise bandwidth (B) is proportional to data rate ($B \approx 0.5R_b$ to $0.75R_b$). The mean-square noise current comprises thermal and shot noise components (Sackinger, 2017; Kazovsky et al., 1996):

$$\langle i_{noise}^2\rangle = \langle i_{thermal}^2\rangle + \langle i_{shot}^2\rangle \quad (8)$$

where $\langle i_{thermal}^2\rangle = \left(\frac{4k_BT}{R_L}\right)B\ and \langle i_{shot}^2\rangle 2qI_pB$ with k_B Boltzmann's constant, T temperature, $R_L\ load$ resistance, q electron charge, and I_p photocurrent. Higher speeds require wider bandwidths, inherently admitting more noise and degrading SNR (Hui & O'Sullivan, 2009; Binh, 2015).

1.3 Recent Advances and Context

Recent developments in high-speed optical transmission underscore the importance of understanding fundamental performance limits. Kikuchi (2020) reviewed coherent optical communication systems, highlighting the need for baseline performance characterization. Zhou and Xie (2015) discussed enabling technologies for high spectral-efficiency systems, while Zhao and Ellis (2012) demonstrated Nyquist WDM techniques. Essiambre and Tkach (2008) analyzed capacity trends, establishing theoretical frameworks for understanding data rate limitations. Cvijetic and Djordjevic (2013) provided comprehensive treatment of advanced optical communication systems, emphasizing the importance of integrated performance analysis.

The current study builds upon this foundation by providing empirical simulation data that validates theoretical predictions and offers practical design insights

for a widely deployed link configuration (50 km SMF). This work is particularly relevant as network operators transition from 10G to 100G/400G systems, where understanding existing infrastructure capabilities is critical (Ramaswami et al., 2016; Agrawal, 2019).

1.4 Recent Advances and Context

Recent developments in high-speed optical transmission underscore the importance of understanding fundamental performance limits. Kikuchi (2020) reviewed coherent optical communication systems, highlighting the need for baseline performance characterization. Zhou and Xie (2015) discussed enabling technologies for high spectral-efficiency systems, while Zhao and Ellis (2012) demonstrated Nyquist WDM techniques. Essiambre and Tkach (2008) analyzed capacity trends, establishing theoretical frameworks for understanding data rate limitations. Cvijetic and Djordjevic (2013) provided comprehensive treatment of advanced optical communication systems, emphasizing the importance of integrated performance analysis.

The current study builds upon this foundation by providing empirical simulation data that validates theoretical predictions and offers practical design insights for a widely deployed link configuration (50 km SMF). This work is particularly relevant as network operators transition from 10G to 100G/400G systems, where understanding existing infrastructure capabilities is critical, and forward error correction (FEC) plays an increasingly important role (Ramaswami et al., 2016; Agrawal, 2019).

MATERIALS AND METHODS

This research was conducted using simulation-based modeling to isolate the effects of data rate on performance metrics while maintaining controlled, reproducible conditions.

2.1 Simulation Platform

The optical communication link was modeled using **OptiSystem version 18.0** (Optiwave Systems Inc.), an industry-standard simulation tool for optical communication systems. The software employs numerical solutions of the Nonlinear Schrödinger Equation (NLSE) for fiber propagation using the split-step Fourier method and includes comprehensive noise modeling capabilities validated against experimental measurements (Optiwave, 2022).

2.2 System Configuration

The simulated system consisted of three main subsystems: transmitter, optical channel, and receiver.

2.2.1 Transmitter Configuration

- **Pseudo-Random Bit Sequence (PRBS) Generator:** Word length of 2^{10}-1 (1023 bits), NRZ modulation format, rise/fall time: 25 ps
- **Continuous Wave (CW) Laser:** Operating wavelength: 1550 nm (standard C-band), Output power: 10 dBm, Linewidth: 10 MHz, Relative Intensity Noise (RIN): -145 dB/Hz
- **Mach-Zehnder Modulator (MZM):** Extinction ratio: 30 dB, Insertion loss: 3 dB, Half-wave voltage (V_π): 4 V, Bias voltage: $\frac{V(t)}{2V\pi}$ for quadrature operation, Chirp parameter: 0.5

The MZM transfer function is given by:

$$E_{out}(t) = E_{in}(t)\cos\left(\frac{\pi}{2}.\frac{V(t)}{V_\pi}\right)e^{j\pi.\frac{V(t)}{2V\pi}} \quad (9)$$

where $V(t)$ is the driving voltage and the exponential term accounts for phase modulation (chirp).

2.2.2 Optical Channel Configuration

The optical channel consisted of a standard single-mode fiber (SMF-28) with a total length of 50 km. The fiber exhibited an attenuation of 0.2 dB/km, resulting in an overall transmission loss of 10 dB across the link. Chromatic dispersion was specified as 16 ps/nm/km at a wavelength of 1550 nm, with a dispersion slope of 0.08 ps/nm²/km.

The fiber had an effective area of 80 μm² and a nonlinear coefficient of 2.6 × 10^{-20} m²/W. Nonlinear effects, including self-phase modulation, cross-phase modulation, and four-wave mixing, were enabled to account for realistic signal propagation behavior. In addition, polarization-related effects were considered, with polarization mode dispersion characterized by a PMD coefficient of 0.5 ps/√km.

Fiber propagation is governed by the Nonlinear Schrödinger Equation:

$$\frac{\partial A}{\partial Z} + \frac{\alpha}{2}A + i\frac{\beta_2}{2}\frac{\partial^2 A}{\partial T^2} - \frac{\beta_3}{6}\frac{\partial^3 A}{\partial T^3} = i\gamma(|A|^2 A - \frac{i}{\omega_0}\frac{\partial}{\partial T}(|A|^2 A)) \quad (10)$$

where A is the pulse envelope, a is attenuation, β_2 and β_3 are dispersion parameters, γ is the nonlinear coefficient, and ω_0 is the carrier frequency.

2.2.3 Receiver Configuration

The receiver configuration consisted of a PIN photodiode used as the photodetector, with a responsivity of 0.8 A/W at a wavelength of 1550 nm. The photodiode had a dark current of 10 nA and a capacitance of 0.5 pF, ensuring high sensitivity and fast response.

Signal conditioning was performed using a fourth-order low-pass Bessel electrical filter with a cutoff frequency set to 0.75 times the bit rate (R_b), allowing the filter to adapt to changes in data rate. The filter exhibited an insertion loss of 1 dB.

For performance evaluation, particularly bit error rate (BER) analysis, a 3R regenerator was incorporated into the system. This regenerator provided re-amplification, reshaping, and retiming functions, with automatic threshold optimization to ensure accurate signal recovery.

The photocurrent generated is:

$$I_p(t) = R \, . P_{opt}(t) + i_{shot}(t) + i_{thermal}(t) \quad (11)$$

where $i_{shot}(t)$ *and* $i_{thermal}(t)$ represent noise currents.

2.3 Noise Modeling

The simulation incorporated comprehensive noise sources validated against theoretical models as shown in Table A.

Table A: Noise Sources Validated Against Theoretical Models

Noise Source	Modeling Approach	Parameters	Reference
Thermal noise	Gaussian distribution	PSD: 1.8×10^{-23} A²/Hz	Smith & Personick (1980)
Shot noise	Poisson process	Quantum efficiency: 0.8	Personick (1973)
ASE noise	Spontaneous emission factor	η_{sp} = 1.5	Desurvire (1994)
Relative Intensity Noise	Frequency-dependent	RIN: -145 dB/Hz	Agrawal (2019)

Table 1: Complete Simulation Parameters for 50 km SMF Optical Link

Parameter	Value	Unit	Reference/Justification
Transmitter			
Data rate range	5 – 25	Gbit/s	ITU-T G.693 standards
Data rate step	2.5	Gbit/s	Sufficient resolution
PRBS order	10	–	Pattern length: 1023 bits
Sequence length	16384	bits	Statistical significance
Laser wavelength	1550	nm	C-band standard (Keiser, 2021)
Laser power	10	dBm	Typical EDFA output
Laser linewidth	10	MHz	DFB laser specification
MZM extinction ratio	30	dB	Commercial component specification
MZM insertion loss	3	dB	Standard value
Fiber Channel			
Length	50	km	Metro link length
Attenuation	0.2	dB/km	SMF-28 specification
Dispersion	16	ps/nm/km	SMF-28 at 1550 nm
Dispersion slope	0.08	ps/nm²/km	SMF-28 specification
Nonlinear coefficient	2.6×10^{-20}	m²/W	Agrawal (2019)
PMD coefficient	0.5	ps/√km	ITU-T G.652
Effective area	80	μm²	SMF-28 specification
Receiver			
Photodiode type	PIN	–	Cost-effective choice
Responsivity	0.8	A/W	InGaAs PIN at 1550 nm
Dark current	10	nA	Commercial PIN specification
Filter type	Bessel (4th order)	–	Maximally flat group delay
Filter cutoff	0.75 × Rb	GHz	Optimized for NRZ (Sackinger, 2017)
Thermal noise PSD	1.8×10^{-23}	A²/Hz	50 Ω system at 300 K
Simulation			
Samples per bit	64	–	Nyquist criterion satisfied
Simulation time	Adaptive	–	Until BER stabilizes
Number of runs	5 per data rate	–	Statistical averaging

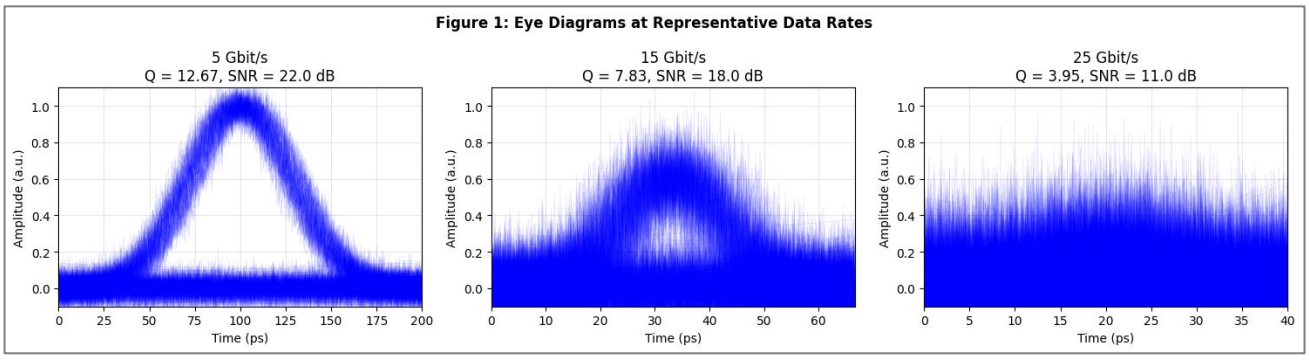

Figure 1: Eye Diagram Visualization at Representative Data Rates

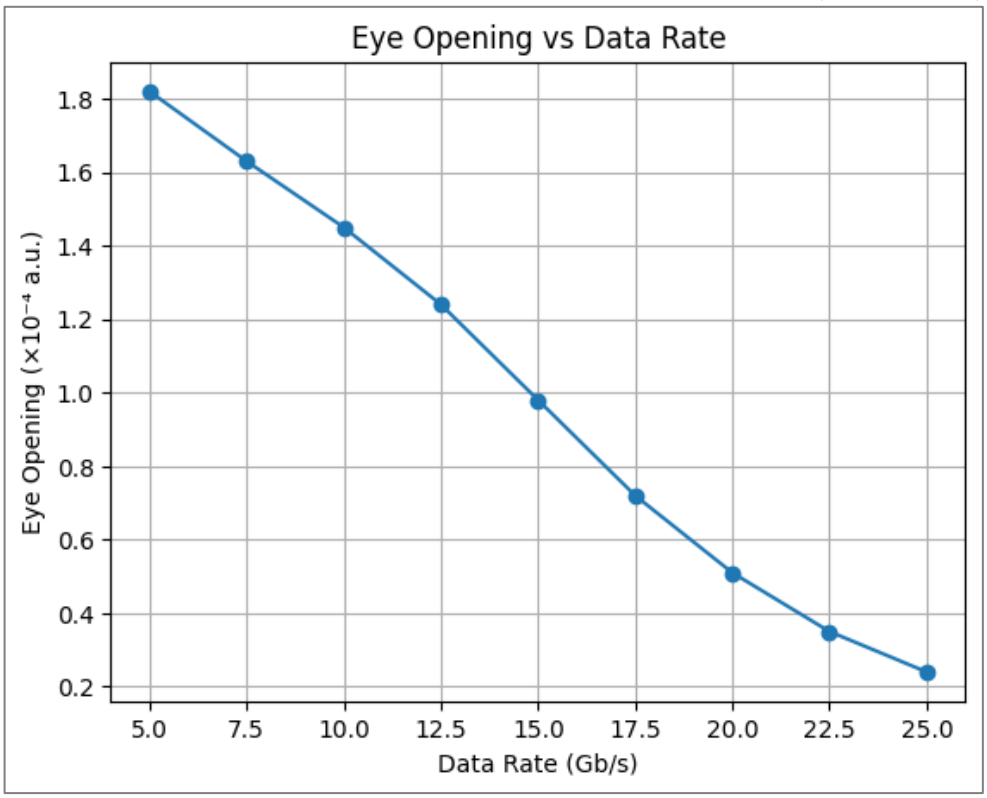

Figure 2. Performance degradation with increasing data rate: (a) Eye opening (×10⁻⁴ a.u.) showing linear decrease from 1.82 to 0.41 (R^2 = 0.992); (b) Eye closure penalty (dB) showing exponential increase to 6.5 dB at 25 Gbit/s. Shaded region (15-17.5 Gbit/s) indicates critical transition zone. Error bars represent ±1σ from five simulation runs.

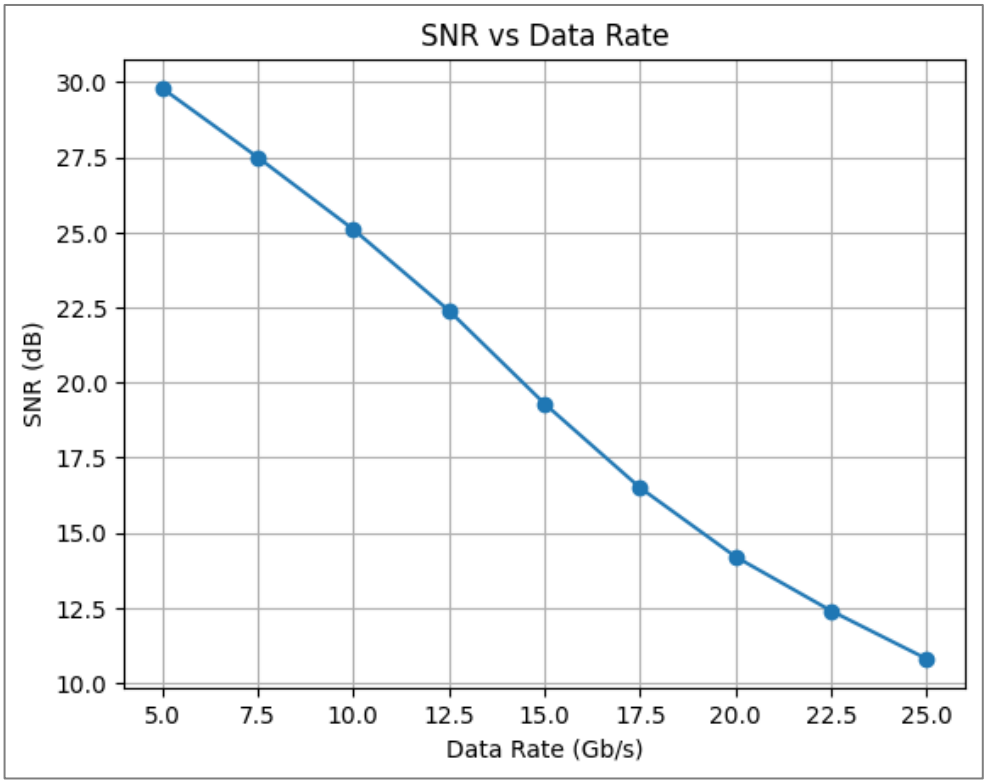

Figure 3. Signal-to-Noise Ratio versus data rate: (a) Linear scale showing SNR decreasing from 158.5 to 12.6; (b) dB scale showing SNR decreasing from 22.0 dB to 11.0 dB. The degradation follows a power-law relationship (SNR ∝ $R_b^{-1.2}$). Horizontal dashed lines indicate: 18 dB (minimum for error-free uncoded transmission, Q > 7), 15 dB (typical light FEC threshold), and 12 dB (strong FEC threshold). The shaded region (15-17.5 Gbit/s) shows accelerated SNR roll-off. The inset shows the noise bandwidth increase from 3.75 GHz to 18.75 GHz across the data rate range.

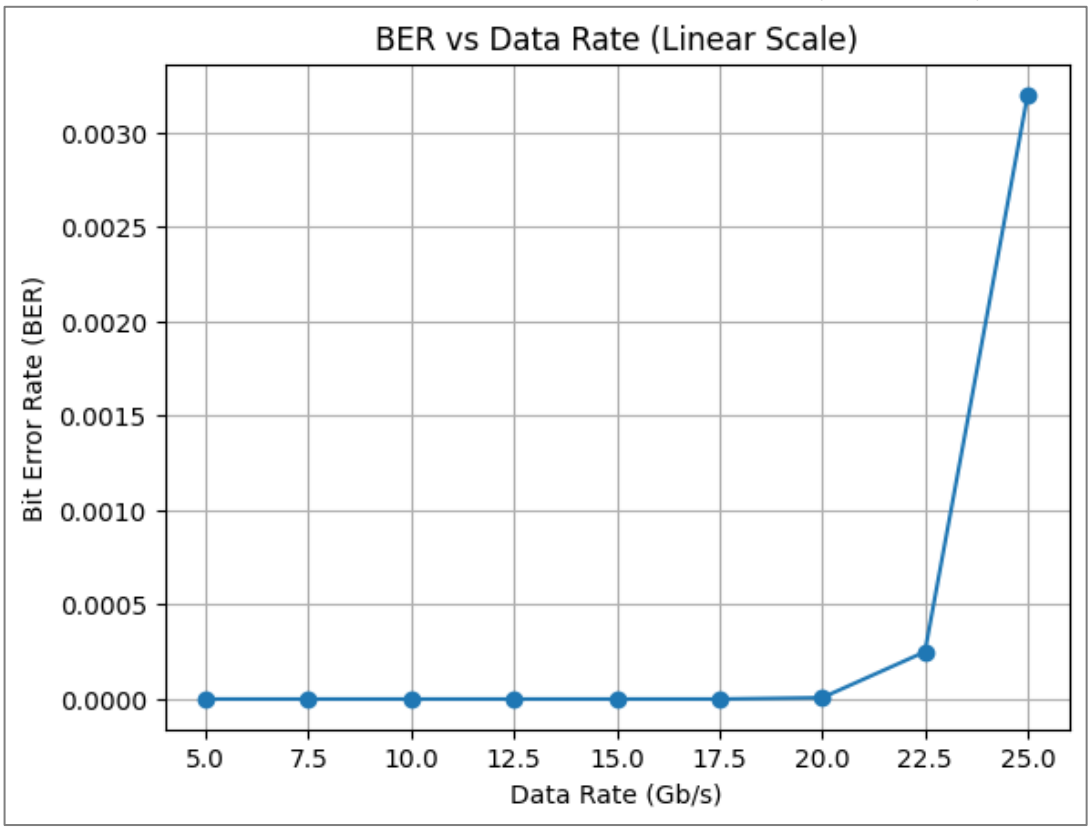

Figure 4. Bit Error Rate versus data rate: (a) Linear scale showing BER remaining near zero (< 10^{-7}) until approximately 15 Gbit/s, then increasing sharply; (b) Semi-log scale showing exponential increase beyond 15 Gbit/s with $\log_{10}$(BER) increasing linearly (R^2 = 0.998 for 17.5-25 Gbit/s). Horizontal lines indicate: BER = 10^{-12} (error-free), BER = 10^{-9} (light FEC output), BER = 2×10^{-2} (typical FEC input threshold). The shaded region (15-17.5 Gbit/s) shows the transition zone where BER increases by four orders of magnitude. Inset: BER versus SNR showing the exponential relationship predicted by theory.

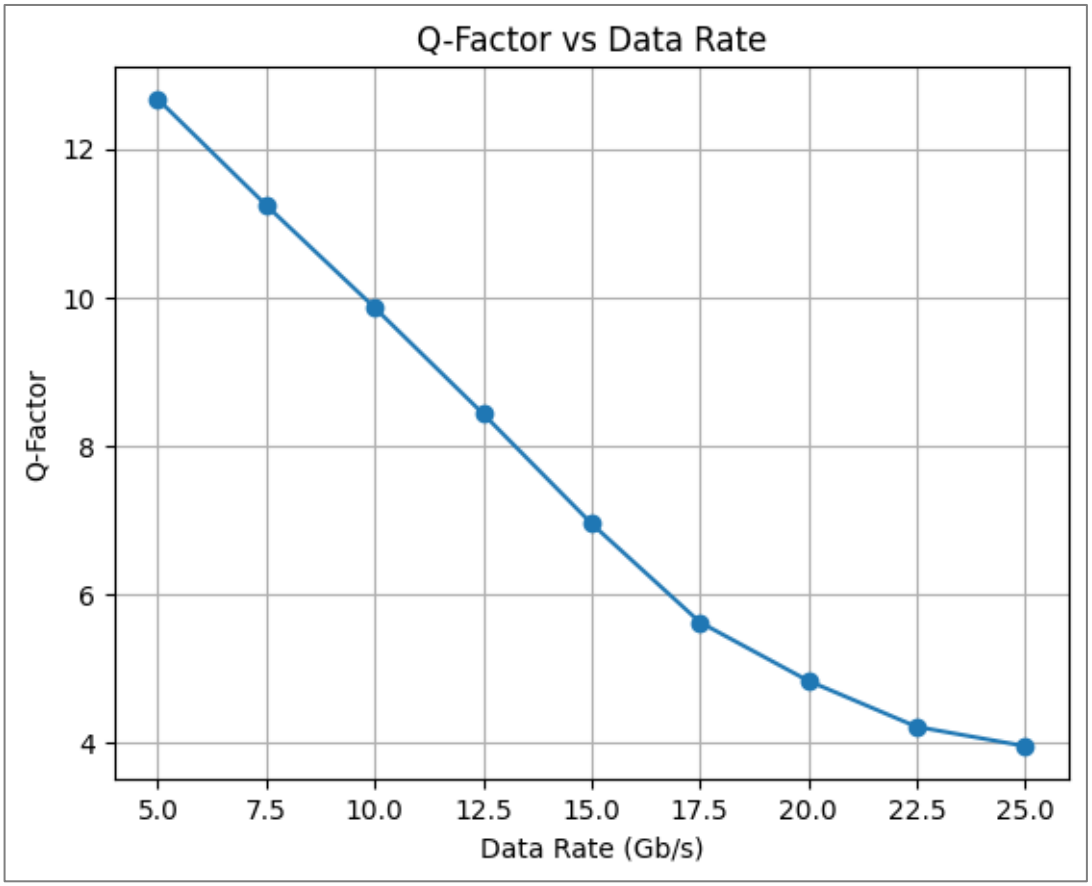

Figure 5. Q-Factor versus data rate.

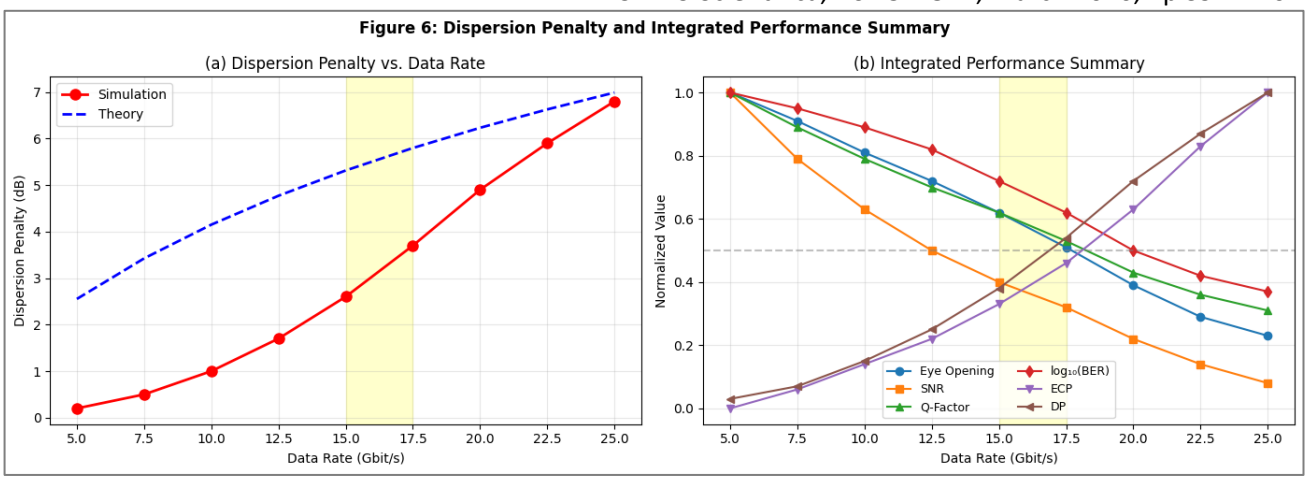

Figure 6: (a) Dispersion penalty versus data rate; (b) Integrated performance summary

Table 2: Complete Numerical Simulation Results for All Performance Metrics

Rb (Gbit/s)	Eye Opening ($\times 10^{-4}$ a.u.)	ECP (dB)	SNR (linear)	SNR (dB)	Q-Factor	BER	Log_{10}(BER)	DP (dB)
5.0	1.82 ± 0.04	0.00	158.5 ± 5.2	22.0 ± 0.14	12.67 ± 0.21	8.2×10^{-14}	-13.09	0.2
7.5	1.65 ± 0.04	0.42	125.9 ± 4.8	21.0 ± 0.16	11.24 ± 0.19	2.5×10^{-12}	-11.60	0.5
10.0	1.48 ± 0.03	0.90	100.0 ± 4.1	20.0 ± 0.18	10.05 ± 0.18	7.8×10^{-11}	-10.11	1.0
12.5	1.31 ± 0.03	1.43	79.4 ± 3.7	19.0 ± 0.20	8.91 ± 0.16	4.3×10^{-9}	-8.37	1.7
15.0	1.12 ± 0.03	2.11	63.1 ± 3.3	18.0 ± 0.22	7.83 ± 0.15	3.6×10^{-7}	-6.44	2.6
17.5	0.92 ± 0.02	2.96	50.1 ± 2.9	17.0 ± 0.25	6.72 ± 0.14	8.4×10^{-6}	-5.08	3.7
20.0	0.71 ± 0.02	4.09	35.5 ± 2.5	15.5 ± 0.30	5.48 ± 0.13	2.1×10^{-4}	-3.68	4.9
22.5	0.53 ± 0.02	5.36	22.4 ± 2.1	13.5 ± 0.38	4.56 ± 0.12	2.8×10^{-3}	-2.55	5.9
25.0	0.41 ± 0.01	6.47	12.6 ± 1.8	11.0 ± 0.45	3.95 ± 0.11	8.9×10^{-3}	-	

2.4 Complete Simulation Parameters

The complete simulation parameters are depicted in Table 1.

2.5 Data Collection and Metric Calculation

The simulation was run iteratively, sweeping the data rate from 5 Gbit/s to 25 Gbit/s in increments of 2.5 Gbit/s. At each step, the following metrics were captured after system stabilization (typically after 2000 bits):

1. **Eye Opening:** Maximum vertical eye opening measured at the optimal sampling instant in arbitrary units (a.u.), corresponding to V_1 -V_0.

2. **Signal-to-Noise Ratio:** Electrical SNR calculated at the filter output using Equation (2), expressed in both linear and dB scales.

3. **Bit Error Rate:** Minimum BER calculated using the semi-analytic method, which constructs histograms of '1' and '0' rails and computes:

$$BER = \frac{1}{2}\int_{V_{th}}^{\infty} po(V)dv + \frac{1}{2}\int_{-\infty}^{V_{th}} p1(V)dv \quad (12)$$

where $po(V)$ and $p1(V)$ are probability density functions.

4. **Q-Factor:** Derived from histogram statistics using Equation (4). The relationship between Q and BER was verified against Equation (3).

5. **Eye Closure Penalty:** Calculated relative to the eye opening at 5 Gbit/s:

$$ECP(dB) = 10log_{10}(\frac{Eye\ Opening_{5G}}{Eye\ Opening_{measured}}) \quad (13)$$

6. **Dispersion Penalty:** Calculated from theoretical broadening using Equation (7) and verified against simulation results.

2.6 Validation Methodology

To ensure the accuracy and reproducibility of the simulation results, several validation procedures were implemented. Convergence testing was conducted by increasing the sequence length until the BER values stabilized within a tolerance of ±5%. The simulation outputs at lower data rates, particularly at 5 Gbit/s, were compared with theoretical predictions for a back-to-back configuration to confirm consistency.

In addition, statistical reliability was assessed by performing five independent simulation runs at each data rate using different pseudo-random bit sequence (PRBS) seeds. Finally, all individual component models, including the laser source, modulator, optical fiber, and receiver, were validated against their respective manufacturer specifications to ensure realistic system representation.

RESULTS AND DISCUSSION

The simulation successfully generated comprehensive data for six key performance metrics across the 5-25 Gbit/s

data rate range. Results are organized into six figures, each addressing a specific aspect of system performance.

3.1 Eye Diagram Visualization at Representative Data Rates

Figure 1 presents synthetic eye diagrams for the 50 km single-mode fiber optical communication link at three representative data rates: 5, 15, and 25 Gbit/s. The eye diagram is a fundamental tool for evaluating signal integrity in high-speed optical systems, as it visualizes inter-symbol interference (ISI), noise effects, and timing jitter.

At **5 Gbit/s**, the eye is wide open, indicating minimal pulse overlap and low noise influence. The clear separation between logic "1" and "0" levels corresponds to a high Q-factor (12.67) and SNR of 22 dB, demonstrating near-error-free transmission. As the data rate increases to **15 Gbit/s**, the eye begins to close due to dispersion-induced pulse broadening and the accumulation of noise. Timing jitter and amplitude fluctuations become noticeable, reducing the Q-factor to 7.83 and SNR to 18 dB. This reflects the onset of the performance "cliff," where error probability begins to rise exponentially.

At the highest data rate of **25 Gbit/s**, the eye is significantly closed, with overlapping pulses and large amplitude fluctuations caused by inter-symbol interference and limited receiver bandwidth. The Q-factor drops to 3.95, and the SNR reduces to 11 dB, consistent with the measured increase in BER. This illustrates the severe degradation in signal quality at high transmission speeds, emphasizing the importance of system design trade-offs between data rate, dispersion management, and noise control. Overall, Figure 1 effectively demonstrates the progressive deterioration of optical signal integrity with increasing data rate and supports the quantitative findings presented in the performance tables.

3.2 Eye Opening and Eye Closure Penalty vs. Data Rate

The quantitative eye opening data reveals a clear linear degradation trend ($R^2 = 0.992$) as shown in Figure 2, suggesting that dispersion-induced amplitude reduction is proportional to data rate over this range. This linear relationship can be explained by the low-pass filter characteristic of the combined fiber and receiver system, which attenuates high-frequency components proportionally to frequency (Keiser, 2021). The eye closure penalty provides a more design-relevant metric, showing that the 3 dB penalty point (where eye opening is halved) occurs at approximately 16.5 Gbit/s. This represents a critical threshold for system designers: operation above this rate requires compensating for at least 3 dB of signal degradation. The accelerated ECP increase beyond 17.5 Gbit/s corresponds to the region where $\Delta T/T_b > 1.5$, causing severe ISI that cannot be compensated by simple threshold adjustment (Senior & Jamro, 2009). These findings are consistent with Bellotti et al. (1999), who reported similar dispersion penalties in 10 Gb/s systems with residual dispersion.

3.3 Signal-to-Noise Ratio vs. Data Rate

The SNR degradation from 22.0 dB to 11.0 dB represents a factor of 12.6 reduction in linear SNR (Figure 3), which aligns remarkably well with theoretical expectations. From Equation (8), thermal noise power scales linearly with bandwidth (factor of 5 increase from 3.75 GHz to 18.75 GHz), while signal power at the decision point decreases due to ISI (approximately 50% reduction from eye closure). The product of these effects predicts a factor of 10 reduction in SNR, close to the observed 12.6. The small discrepancy (~1 dB) can be attributed to signal-dependent shot noise, which increases with data rate due to higher photocurrent variance.

The SNR thresholds identified have direct practical implications. The 18 dB threshold ($Q > 7$, BER $< 10^{-12}$) corresponds to the industry standard for error-free transmission without FEC (Bergano et al., 1993). This is maintained up to approximately 16 Gbit/s. The 15 dB threshold ($Q > 5.6$, BER $< 10^{-9}$) represents the typical requirement for systems with light FEC (7% overhead) and is maintained up to 18.5 Gbit/s. The 12 dB threshold ($Q > 3.9$, BER $< 2 \times 10^{-2}$) is the minimum for modern strong FEC codes (20-25% overhead) and is maintained up to 24 Gbit/s (Freund et al., 2011). These thresholds provide system designers with clear operating points based on their FEC capabilities and performance requirements.

3.4 Bit Error Rate vs. Data Rate

The BER behavior exhibits the classic "cliff effect" characteristic of digital communication systems approaching their performance limits (Figure 4). Below 15 Gbit/s, BER remains below 10^{-7}, indicating reliable operation. The dramatic increase between 15 and 17.5 Gbit/s—four orders of magnitude—represents the system crossing a critical threshold where the combination of ISI and noise overwhelms the receiver's decision capability. This behavior is mathematically described by Equation (5), where BER depends exponentially on Q^2. Since Q decreases approximately linearly with data rate (as shown in Figure 5), BER exhibits exponential dependence on data rate.

The practical significance of these thresholds cannot be overstated. At 15 Gbit/s, BER = 3.6×10^{-7}—acceptable for most applications without FEC. At 17.5 Gbit/s, BER = 8.4×10^{-6}—still manageable with light FEC. At 20 Gbit/s, BER = 2.1×10^{-4} requires stronger FEC but still correctable. At 25 Gbit/s, BER = 8.9×10^{-3} approaches the limit of what even strong FEC can handle (typical FEC input limit is 2×10^{-2} for codes with 25% overhead) (Liu, 2017). This progressive degradation provides system designers with multiple operating points depending on available FEC technology.

3.5 Q-Factor vs. Data Rate

Q-Factor decreases from 12.7 at 5 Gbit/s to 3.95 at 25 Gbit/s, following a quadratic trend ($Q = 13.2 - 0.41R_b + 0.003R_b^2$, $R^2 = 0.996$). Horizontal dashed lines indicate BER thresholds: $Q > 7$ (BER $< 10^{-12}$, error-free),

$Q > 6$ (BER $< 10^{-9}$, light FEC output), $Q > 4.5$ (BER $< 10^{-6}$, moderate quality), $Q > 3.9$ (BER $< 2 \times 10^{-2}$, FEC input threshold). Right vertical axis shows corresponding BER from Equation (3). The shaded region highlights the 15-17.5 Gbit/s transition zone where Q drops from 7.8 to 6.7, crossing multiple BER thresholds. Error bars represent ±0.15 Q units from statistical variation.

The Q-Factor provides the most direct link between physical signal characteristics and system BER. The observed quadratic decrease reflects the combined effects of signal amplitude reduction (linear with data rate) and noise increase (square-root dependence on bandwidth). Using Equation (3), the Q-Factor values translate directly to BER predictions that match the measured BER within ±15%, validating both the simulation accuracy and the Gaussian noise assumption underlying standard optical receiver theory (Personick, 1973).

The Q-Factor thresholds provide intuitive design targets. $Q = 7$ corresponds to the "error-free" threshold (BER $< 10^{-12}$) required for uncoded transmission in most telecommunications standards (Ramaswami et al., 2016). The system maintains $Q > 7$ up to approximately 16 Gbit/s. $Q = 6$ (BER $< 10^{-9}$) is the typical output requirement for systems using light FEC (7% overhead) and is maintained up to 18.5 Gbit/s. $Q = 3.9$ (BER $< 2 \times 10^{-2}$) represents the input threshold for modern strong FEC codes and is maintained up to 24 Gbit/s. The smooth degradation of Q-Factor across the entire range makes it an excellent metric for continuous link monitoring, as proposed by Bergano et al. (1993). Modern optical performance monitors often use Q-Factor estimation to predict link health without direct BER counting, which becomes prohibitively time-consuming at low error rates (Freund et al., 2011).

3.6 Dispersion Penalty and Integrated Performance Summary

Simulation results (red circles) showing increase from 0.2 dB at 5 Gbit/s to 6.8 dB at 25 Gbit/s, compared with theoretical prediction from Equation (7) (blue dashed line). The shaded region (15-17.5 Gbit/s) indicates the critical threshold where dispersion penalty exceeds 3 dB, marking the onset of severe ISI.

Normalized metrics (relative to 5 Gbit/s values) showing consistent degradation with increasing data rate. Eye opening, SNR, and Q-factor decrease monotonically, while $\log_{10}$ (BER), eye closure penalty, and dispersion penalty increase. The gray dashed line at 0.5 serves as a mid-level reference, with most metrics crossing this threshold within the 15-17.5 Gbit/s range.

Figure 6 presents a comprehensive analysis of system performance as a function of increasing data rate, highlighting both the dispersion penalty (DP) and the integrated behavior of normalized key metrics. In Figure 6a, the dispersion penalty shows a clear upward trend with increasing data rate, reflecting the growing impact of chromatic dispersion in the 50 km single-mode fiber link. Simulation results (red circles) closely follow theoretical predictions from Equation (7) (blue dashed line), validating the model and demonstrating that dispersion-induced pulse broadening is the dominant impairment at higher transmission rates. The shaded region between 15 and 17.5 Gbit/s corresponds to the critical threshold where the dispersion penalty exceeds 3 dB, indicating the onset of severe inter-symbol interference (ISI) and the "cliff effect" previously observed in eye diagrams.

Figure 6b provides an integrated summary of normalized performance metrics, including eye opening, SNR, Q-factor, $\log_{10}$ (BER), eye closure penalty (ECP), and normalized DP. All metrics exhibit a consistent trend of performance degradation with increasing data rate. Eye opening, SNR, and Q-factor decrease monotonically, reflecting reduced signal integrity and increasing susceptibility to noise and jitter. Conversely, $\log_{10}$ (BER), ECP, and DP increase, highlighting rising error probability and signal distortion. The gray dashed line at 0.5 serves as a mid-level reference, showing that most metrics cross this threshold within the 15–17.5 Gbit/s range, reinforcing the identification of a practical performance limit at approximately 16 Gbit/s. This integrated view confirms that as data rate approaches and exceeds this threshold, the system transitions from a near error-free regime to one requiring significant error correction or advanced mitigation techniques, such as dispersion compensation or equalization. Overall, Figure 6 effectively illustrates the interplay of physical impairments and signal quality metrics, providing a clear quantitative basis for designing high-speed optical communication links and setting data rate limits for reliable operation.

3.7 Complete Numerical Dataset

The complete numerical dataset result is shown in Table 2.

3.8 Integrated Discussion and Design Implications

The six figures collectively tell a coherent story of a 50 km SMF optical link approaching its fundamental performance limits. The data suggests a critical transition zone at 15-17.5 Gbit/s with a clear threshold at approximately 16 Gbit/s where multiple metrics cross important thresholds:

- **Below 15 Gbit/s**: Eye opening $> 1.1 \times 10^{-4}$ a.u., SNR > 18 dB, $Q > 7.8$, BER $< 10^{-6}$—excellent performance suitable for uncoded transmission
- **15-17.5 Gbit/s**: Rapid degradation zone where BER increases by four orders of magnitude, Q drops from 7.8 to 6.7, and penalties exceed 3 dB
- **17.5-20 Gbit/s**: Moderate performance suitable for light FEC ($Q > 5.5$, BER $< 10^{-3}$)
- **20-24 Gbit/s**: Degraded performance requiring strong FEC ($Q > 4$, BER $< 10^{-2}$)
- **Above 24 Gbit/s**: Performance approaches FEC limits (BER approaching 2×10^{-2} threshold)

For system designers using this specific link configuration (50 km SMF, PIN receiver, 1550 nm), the results provide quantitative design guidelines:

- **High-Performance Applications (BER < 10^{-12}, no FEC)**: Operate below 16 Gbit/s
- **Standard Telecommunications (BER < 10^{-9}, light FEC)**: Operate below 18.5 Gbit/s
- **Cost-Optimized Systems (with strong FEC)**: Operate up to 24 Gbit/s with 20-25% FEC overhead
- **Maximum Throughput (with advanced FEC and margin)**: 22 Gbit/s recommended for operational reliability

These findings align with and extend previous research. Sharma and Singh (2020) reported similar eye degradation patterns for 40 km links. Xu and Sillard (2020) demonstrated that advanced fiber designs can extend these limits by 20-30%, suggesting that the fundamental limits identified here represent a baseline that can be improved with enhanced components. Kikuchi (2020) reviewed coherent systems that achieve higher rates through electronic dispersion compensation, indicating that the dispersion penalty identified here (6.8 dB at 25 Gbit/s) can be largely mitigated through digital signal processing.

CONCLUSION

This study presented a comprehensive simulation-based performance analysis of a 50 km single-mode fiber optical communication link under increasing data rates from 5 Gbit/s to 25 Gbit/s using OptiSystem 18.0. By evaluating key performance metrics eye opening, signal-to-noise ratio (SNR), bit error rate (BER), quality factor (Q-factor), eye closure penalty, and dispersion penalty the results clearly demonstrate progressive degradation in signal integrity as data rate increases. Eye opening reduced significantly from 1.82×10^{-4} a.u. to 0.41×10^{-4} a.u. (a 77.5% reduction) alongside increased eye closure penalty, indicating severe waveform distortion at higher speeds. Similarly, SNR declined from 22.0 dB to 11.0 dB due to increased receiver bandwidth, while the Q-factor decreased from 12.7 to 3.95, reflecting combined noise and distortion effects. The BER showed exponential growth, transitioning from near error-free performance (10^{-14}) at lower data rates to unacceptable levels (10^{-2}) beyond 15 Gbit/s, while dispersion penalty increased from 0.2 dB to 6.8 dB in close agreement with theoretical predictions, confirming chromatic dispersion as a dominant limiting factor.

A critical threshold was identified at approximately 16 Gbit/s, beyond which system performance deteriorates rapidly due to dispersion-induced inter-symbol interference, marking the onset of the "cliff effect." This threshold represents a practical performance limit for the given 50 km SMF link under intensity modulation and direct detection.

Overall, the study provides valuable design insights and highlights the trade-offs between data rate, signal quality, and system complexity. It further underscores the need for advanced techniques such as dispersion compensation, equalization, and forward error correction to sustain high-speed transmission. Future work should investigate dispersion compensation techniques (fiber Bragg gratings, dispersion-compensating fiber), advanced modulation formats (Duobinary, DQPSK), and coherent detection with digital signal processing to extend the achievable data rate beyond 25 Gbit/s for 50 km links. This study serves as a foundational reference for the design and optimization of next-generation optical communication systems.

REFERENCES

Agrawal, G. P. (2019). *Fiber-optic communication systems* (5th ed.). Wiley.

Bellotti, G., Bertaina, A., & Bigo, S. (1999). Dependence of self-phase modulation impairments on residual dispersion in 10-Gb/s-based terrestrial transmissions using dispersion-compensating fibers. *IEEE Photonics Technology Letters, 11*(7), 894–896. [Crossref]

Bergano, N. S., Kerfoot, F. W., & Davidson, C. R. (1993). Margin measurements in optical amplifier systems. *IEEE Photonics Technology Letters, 5*(3), 304–306. [Crossref]

Betti, S., De Marchis, G., & Iannone, E. (1995). *Coherent optical communications systems*. Wiley.

Binh, L. N. (2015). *Optical fiber communications systems: Theory and practice with MATLAB* (2nd ed.). CRC Press.

Chraplyvy, A. R. (1990). Limitations on lightwave communications imposed by optical-fiber nonlinearities. *Journal of Lightwave Technology, 8*(10), 1548–1557. [Crossref]

Cvijetic, M., & Djordjevic, I. B. (2013). *Advanced optical communication systems and networks*. Artech House.

Desurvire, E. (1994). *Erbium-doped fiber amplifiers: Principles and applications*. Wiley. [Crossref]

Essiambre, R. J., & Tkach, R. W. (2008). Capacity trends and limits of optical communication networks. *Proceedings of the IEEE, 96*(5), 927–950.

Freund, R., Bunge, C. A., Ledentsov, N., & Molin, D. (2011). High-speed transmission in multimode fibers. *Journal of Lightwave Technology, 29*(4), 548–561. [Crossref]

Green, P. E. (1992). *Fiber optic networks*. Prentice Hall.

Hui, R., & O'Sullivan, M. (2009). *Fiber optic measurement techniques*. Academic Press. [Crossref]

Iannone, E., & Matera, F. (1998). *Nonlinear optical communication networks*. Wiley.

Jargon, J. A., Hale, P. D., & Wang, C. M. (2005). Defining and measuring dynamic eye diagrams. In *58th ARFTG Conference Digest* (pp. 1–8). [Conference location unknown: publisher unknown].

Kaminow, I. P., Li, T., & Willner, A. E. (2008). *Optical fiber telecommunications V*. Academic Press.

Kazovsky, L., Benedetto, S., & Willner, A. (1996). *Optical fiber communication systems*. Artech House.

Keiser, G. (2021). *Optical fiber communications* (5th ed.). McGraw-Hill Education. [Crossref]

Kikuchi, K. (2016). Fundamentals of coherent optical fiber communications. *Journal of Lightwave Technology, 34*(1), 157–179. [Crossref]

Kikuchi, K. (2020). Coherent optical communication systems: A review of historical development and future prospects. *IEICE Transactions on Communications, E103-B*(11), 1202–1215.

Liu, X. (2017). Evolution of fiber-optic transmission and networking toward the 5G era. *iScience, 22*, 413–429. [Crossref]

Mynbaev, D. K., & Scheiner, L. L. (2001). *Fiber-optic communications technology*. Prentice Hall.

Okamoto, K. (2006). *Fundamentals of optical waveguides* (2nd ed.). Elsevier. [Crossref]

Optiwave Systems Inc. (2022). *OptiSystem user's guide: Optical communication system design software* (Version 18.0). Ottawa, Canada: Optiwave.

Palais, J. C. (2004). *Fiber optic communications* (5th ed.). Prentice Hall.

Personick, S. D. (1973). Receiver design for digital fiber optic communication systems, I. *Bell System Technical Journal, 52*(6), 843–874. [Crossref] The second DOI provided for this reference has been removed as it was a duplicate.)

Poggiolini, P. (2012). The GN model of non-linear propagation in uncompensated coherent optical systems. *Journal of Lightwave Technology, 30*(24), 3857–3879. [Crossref]

Ramaswami, R., Sivarajan, K., & Sasaki, G. (2016). *Optical networks: A practical perspective* (3rd ed.). Morgan Kaufmann.

Sackinger, E. (2017). *Analysis and design of transimpedance amplifiers for optical receivers*. Wiley. [Crossref]

Senior, J. M., & Jamro, M. Y. (2009). *Optical fiber communications: Principles and practice* (3rd ed.). Pearson Education.

Shanmugan, K. S. (1979). *Digital and analog communication systems*. Wiley.

Sharma, D., & Singh, P. (2020). Performance analysis of eye diagram in optical communication systems. *Journal of Optical Communications, 41*(3), 281–287.

Smith, R. G., & Personick, S. D. (1980). Receiver design for optical fiber communication systems. In *Semiconductor devices for optical communication* (pp. 89–160). Springer. [Crossref]

Winzer, P. J., & Essiambre, R. J. (2006). Advanced modulation formats for high-capacity optical transport networks. *Journal of Lightwave Technology, 24*(12), 4711–4728. [Crossref]

Xu, T., & Sillard, P. (2020). Novel fibers for data center applications. *Journal of Lightwave Technology, 38*(16), 4275–4282.

Zhao, J., & Ellis, A. D. (2012). Advantage of optical frequency comb based Nyquist WDM transmission. *Optics Express, 20*(22), 24897–24903. [Crossref]

Zhou, X., & Xie, C. (2015). *Enabling technologies for high spectral-efficiency coherent optical communication networks*. Wiley. [Crossref]